Hindawi
Geofluids
Volume 2022, Article ID 9151766, 11 pages
https://doi.org/10.1155/2022/9151766

Research Article

Investigation on Pressure Relief and Roadway Protection Technology by Subsection Hydraulic Fracturing under Strong Mining Pressure in Fully Mechanized Mining

Yingjie Liu[1,2]

[1]*Chinese Institute of Coal Science, Beijing 100013, China*
[2]*Guoneng Shendong Coal Group Corporation Ltd., 719315, China*

Correspondence should be addressed to Yingjie Liu; 290783585@qq.com

Received 6 May 2022; Accepted 26 July 2022; Published 11 August 2022

Academic Editor: Yingfeng Sun

In this study, we analyzed the deformation and stress changes of an auxiliary transport gateway in Buertai coal mine 42106, which is a fully mechanized coal face. We used the directional long drilling hydraulic fracturing technology to weaken the mine hard roof clearance and investigated the overall pressure characteristics of the working face, mining, and two consecutive roadway surrounding rock deformations. The analysis showed that the segmented hydraulic fracturing technology of directional long drilling decreased the pressure in the area affected by the fracturing drilling on the working face after fracturing. The peak pressure decreased by approximately 10.4%, average resistance of the stent was reduced by 2.6%, average resistance of the support decreased by 6.8% under pressure, and dynamic load coefficient decreased by 4%. Furthermore, the roadway deformation decreased, and the coal face was restrained. The stress monitoring value of the surrounding rock was weakened, demonstrating the effectiveness of the fracturing weakening effect.

1. Introduction

Hydraulic fracturing technology was introduced in China in the 1960s as an effective stimulation technique for oil and gas wells. The technology has evolved into other industries, such as in situ stress measurement, geothermal resource development, and nuclear waste disposal [1–3]. Hydraulic fracturing research was first conducted in the Datong mining area and has been widely applied in aspects such gas permeability improvement [4–7], roof cutting pressure relief [8–11], initial mining and caving [12–15], and rock burst prevention [16–19]. The study of hydraulic fracturing expansion in rock mass has clarified fracture propagation characteristics [20–22] and rock mass failure mechanism [23–25]. With the wide application and development of directional drilling technology in coal mines, hydraulic fracturing and directional drilling technologies have been combined and applied to improve gas reflection on-site in some mining areas. This combination has effectively improved the gas predrainage rate and extraction amount of coal seams [26–29].

The local buried depth of 42 coal seam Shendong Buertai is over 400 m. A hard roof and overlying stress concentrated at the coal pillars increase the dynamic loading pressure of the working face [30, 31]. Mining processes have caused serious mine pressure accidents, such as the crushing of the working face support and bursting of hydraulic cylinders. During secondary mining, the roof is fractured, side and floor drums are severe in a 100 m advancement of the working face roadway, and the roadway is difficult to maintain. Therefore, it is necessary to determine a safe and an efficient way of mining 42 coal [32, 33]. In Buertai coal mine, support strength and short drilling hydraulic fracturing are increased to control strong ore pressure, but the method has not completely solved the problem of a strong ore pressure during mining [34].

As highlighted above, many studies have applied hydraulic fracturing technology in coal mines, but only a few have applied directional long drilling segmented hydraulic fracturing technology in pressure relief and roadway protection. Therefore, we applied the directional long drilling

segmented hydraulic fracturing technology on 42 coal of Shendong Buertai coal mine. We compared and analyzed the ore pressure appearance, stress change, working face deformation, and two gateways before and after directional long drilling fracturing. This work is expected to provide a basis for applying the directional long drilling hydraulic fracturing technology to pressure control in mining thick coal seams.

2. Working Face Overview

Buertai coal mine 42106 is a fully mechanized caving working face, which is in the southeast of the main roadway in the second panel of 42 coal mining area. For the second mining face in the second panel of 42 coal mining area, the working face strike length is 4485.24 m, working face dip length is 320 m, mining height is M, and mining area is 1.4353 m square meters. The southeast side is the 42106 and 42107 goafs, as shown in Figure 1.

42106 working face is affected by strong pressure. A large area of roof pressure occurs at 140 m advance, serious floor heave. (It was affected by a mining, and the secondary wall has been pumped 0.5 m). In advance, 140 m large area roof weighting serious floor heave (vice help has been affected by a mining, drum 0.5 m), the dynamic load appears, mainly for large shaking tail roof, roof fall slag, ahead of 100 m within the scope of return air along the trough bottom floor heave is serious, cause the return air along the trough forepoling indiana is difficult. The dynamic load was severe. The main performance was that the tail roof rattles and the roof dropped slag. The bottom heave of the trough floor of the return air within 100 m advance was serious, which made it difficult to pull the lead support along the groove of return air. The negative drum along the return air groove is about 1.6 m, and the negative mesh package is crowded on the working face support and the tail motor of the transport plane, resulting in the difficulty of pushing and pulling, which affects the normal production. The return air tunnel is affected by the secondary mining and the concentrated stress of the coal pillar in the overlying goaf (layer spacing is 77 m). The surrounding rock deformation of the return air tunnel is serious, and the dynamic pressure phenomenon of the working face is obvious. The negative drum in the return air duct is approximately 1.6 m, and the negative net bag is crowded against the working face support and tail motor of the transport plane, resulting in pushing and pulling difficulty and affecting production. Under the influence of secondary mining and coal pillar concentration stress in the overlying goaf (layer spacing, 77 m), the surrounding rock deformation of the return air roadway is severe, and the working face dynamic pressure is obvious.

3. Design and Application of Directional Long Hole Hydraulic Fracturing

Directional long drilling hydraulic fracturing technology is mainly implemented through the thick roof of coal seams. A step-by-step implementation of the directional long drilling on a thick roof span effectively forms continuous support, reduces the sudden release of energy in the roof, and minimizes the internal stress of the roadway surrounding rock, thereby reducing the strong pressure of the working face caused by the frequency and intensity of mine disasters.

3.1. Hydraulic Fracturing Scheme. Working face mining and overlying coal seam position, such as legacy protection of coal seam position prone to strong position of mine pressure appear problem, put forward the borehole layout, plan layout 3 drilling field, accumulative total 9 drilling, design aperture of 96 mm, the orifice opened 96 mm drilling to direct roof, two opening pipe-expanding 153 mm, and 127 mm casing under 10 m across the rocks. After the casing was completed, we drilled 96 mm into the final hole according to the design track, and the drilling and fracturing target layer was the basic top sandstone of the 42 coal seam. The scheme design is described below.

The scheme contained three drill yards. The first drill yard was 550 m away from the cutting hole and was located in 30 connected lanes of the transport passage of the 42106 working face. The second drill yard was 810 m away from the cutting hole of the working face, and the yard contained 29 connected lanes for transporting materials in the 42106 working face. The third drill yard was 1,950 m away from the working face, and the 42106 working face transport tunnel was located between 23 and 24 lanes.

Each drilling site was equipped with 3 holes (making a total of 9 holes) and a single hole length of 300–530 m (making a cumulative length of 4,015 m). Holes 1-1, 2-1, and 3-1 were located under the remaining protection coal seam of the 22202 working face, and the distance between the holes was 90 m from the transport channel of the 42106 working face. The distance between adjacent holes in the drilling site was 80 m, and the distance between holes 1-3, 2-3, and 3-3 was 70 m from the return air channel of the 42106 working face.

The adjacent holes in the first and second drill yards were designed to be 30 m apart when a single hole is fractured in adjacent locations. When fracturing is required for both boreholes, the spacing between the boreholes should be 60 m. Figure 2 illustrates the initial intensive fracturing conditions of the 42107 working face of the mine, fracturing interval initial design of 30 m, fracturing interval length of 6.5 m, single hole fracturing of 7 stages, total fracturing of 63 stages, and drilling design plan. Table 1 presents the drilling construction parameters.

3.2. Fracturing Data Analysis. Nine fractures were completely drilled in the working face, with 300–450 m^3 of water injected into a single hole and over 2,800 m^3 of injected water in total. The influence range of the fracturing drilling covered the whole working face, with a hole diameter of 96 mm and a length of 330–564 m. The transported fracturing tool strings totaled 3,698.38 m; 74 stages of staged fracturing were performed, with maximum and minimum pressures of 33.1 MPa and 8.6 MPa, respectively. A maximum fracture pressure drop of 12.8 MPa and a pressure drop of over 3 MPa were observed 593 times, forming effective three-dimensional fractures and reducing the overall strength of the roof. Table 2 summarizes the fracturing construction details.

Figure 1: 42106 working face layout.

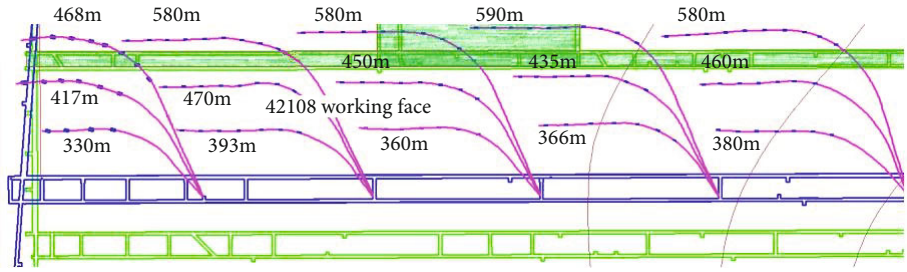

Figure 2: Design plan of fracturing drilling.

Table 1: Drilling construction parameters.

Construction site	Boring number	Drilling field distance from cutting hole/m	Control horizon	Aperture/mm	Drilling long/m	Fracturing section/PCS
No. 1	1-1	550	Packsand	96	390	7
	1-2	550	Packsand	96	445	7
	1-3	550	Packsand	96	500	7
No. 2	2-1	810	Packsand	96	320	7
	2-2	810	Packsand	96	410	7
	2-3	810	Packsand	96	520	7
No. 3	3-1	1950	Packsand	96	430	7
	3-2	1950	Packsand	96	470	7
	3-3	1950	Packsand	96	530	7
Total					4015	63

Table 2: Summary of fracturing drilling data.

Job location	Drilling	Drilling long/m	Tool string installation depth/m	Fracturing section/PCS	Maximum pressure/MPa	Minimum pressure/MPa	Largest pressure drop/MPa	Pressure drop number
No. 30 drilling	SF1	426	424.87	8	25.1	14.1	8.2	74
	SF2	476	468.07	8	25.9	10.9	9.8	56
	SF3	516	502.25	10	29.2	10.6	7	71
No. 29 drilling	SF1	330	318.79	6	30.7	14.7	9.2	47
	SF2	426	420.21	8	28	14.2	7.1	55
	SF3	519	503.55	9	26.9	9.8	10	65
No. 22 drilling	SF1	462	458.85	8	33.1	12.6	12.8	66
	SF2	513	504.32	9	31.3	12.6	8	87
	SF3	564	556.32	8	28.8	8.6	11.8	72
Total		4196		74				593

4. Ore Pressure Characteristics

During the 42106 mining, a mine pressure monitoring system was used for the dynamic monitoring of the roof pressure bracket in the fracturing construction area. By comparing the mine pressure before and after the overall evaluation of the fracturing effect, we determined the main contrast parameters to be the extraction compressive strength, pressure interval, dynamic load coefficient, and roadway roof deformation.

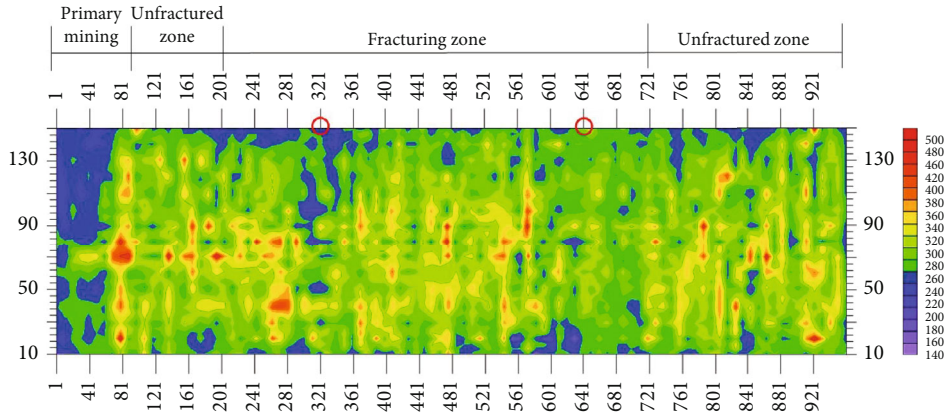

Figure 3: Plane characteristics of ore pressure changes.

Table 3: Analysis of ore pressure evaluation data.

Fracturing status	Pressure step/m	Scope of stents		Hydraulic support at the end of cycle resistance/bar		
				To pressure before	To pressure mean value	Dynamic factor
Not fracturing	21	Periodic weighting 1	40–110	291	422	1.45
	26	Periodic weighting 2	20–80	311	429	1.38
	25	Periodic weighting 3	50–100	285	417	1.46
	23	Periodic weighting 4	30–120	288	421	1.46
	24	Periodic weighting 5	50–110	294	425	1.45
	26	Periodic weighting 6	60–130	281	406	1.44
	20	Periodic weighting 7	20–155	299	405	1.35
	22	Periodic weighting 8	25–110	302	423	1.40
	23	Periodic weighting9	75–125	300	426	1.42
	24	Periodic weighting10	15–110	297	429	1.44
Mean value	23.4	Mean value		294.8	420.3	1.43
Fracturing	19	Periodic weighting 1	30–100	273	385	1.41
	22	Periodic weighting 2	25–90	277	375	1.35
	25	Periodic weighting 3	20–110	286	377	1.32
	24	Periodic weighting 4	35–90	295	390	1.32
	21	Periodic weighting 5	15–130	291	395	1.36
	22	Periodic weighting 6	70–120	288	398	1.38
	22	Periodic weighting 7	15–100	304	406	1.34
	24	Periodic weighting 8	70–120	281	405	1.44
Mean value	22.4	Mean value		286.9	391.4	1.37

4.1. Overall Pressure Characteristics. The results of the downhole tracking monitoring and support data collection were used to plot the change in support resistance in the working position, as shown in Figure 3.

Figure 3 shows that the working face stops at 66 m; the first and average pressures are 588 bar and 301 bar, respectively; and the pressure step is 66 m. Table 3 and Figure 4 show that before entering the frac stage (67–182 m), the maximum periodic pressure was 591 bar, with an average of 344 bar. The periodic pressure step was 44–46 m, and the pressure range was wide. At the frac stage (182–716 m), the maximum periodic pressure was 501 bar, with an average of 311 bar. The periodic pressure interval was 19–25 m, and the overall pressure range was considerably reduced. Beyond the frac stage (716–960 m), the maximum periodic pressure was 597 bar, with an average of 352 bar, and the periodic pressure step was 20–26 m.

4.2. Deformation Condition of Working Face and Two Passageways. Roof movements generate support working resistances and its associated changes. This phenomenon can be used for describing the influence of roof movement on the support working resistance. The dynamic load coefficient (Kd) is the average working resistance of the bracket before pressing divide by the average working resistance of the bracket after pressing. According to the comparison calculation of the support resistance data before and after the working face pressure, in the 182–716 m fracturing area,

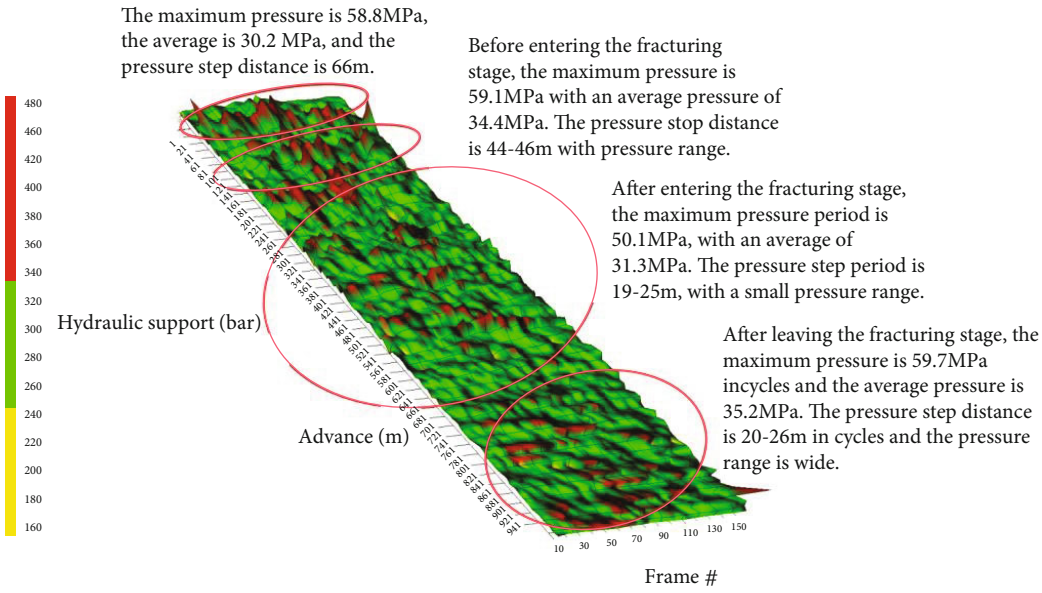

Figure 4: 3D variation characteristics of ore pressure.

the overall dynamic load coefficient was 1.32–1.44, with an average of 1.37, and the overall dynamic load effect was relatively small. During the subsequent pressure period, the coal wall of the working face was relatively complete, the wall was small, and the maximum depth of the wall was 0.5 m. The roof of the aft goaf collapsed in a timely manner, and no hanging roof phenomenon occurred. The auxiliary drum phenomenon of the 42106 auxiliary transport passage was not obvious. In the unfractured area of 716–960 m, the overall dynamic load coefficient was 1.35–1.46, with an average of 1.43, and the overall dynamic load effect was large. The subsequent pressure period was accompanied by the working face wall, and the maximum depth of the wall was 1.0 m. The roof of the tail goaf did not collapse in time.

4.3. Deformation Observation of Roadway Surrounding Rock. At 200 m from the auxiliary roadway of the 42106 fully mechanized caving face to the cutting eye, a measuring point was set at every 100 m, and a total of eight observation points were set at a range of 200–900 m. The cross-point method was adopted for observing section displacement, where point A was in the middle of the roof, point B on the front side, and point D on the secondary side. Points B and D were at the same height. Point C was the intersection with the bottom plate by leading a thin rope from point A in the natural sagging state; points 1–8 corresponded to positions 200–900 m. The maximum relative displacements of the roof, floor, and two sides at each point are plotted as broken line graphs in Figures 5 and 6.

Figures 5 and 6 show that the maximum displacement of the two sides at points 1–6 (200–700 m away from the cutting hole and in the fracturing area of the roof) was 150–200 mm, the maximum displacement of the top and bottom plates was 100–150 mm, and the maximum displacement at points 7 and 8 (800–900 m away from the cutting hole) was 150–200 mm. The maximum displacement of the two sides

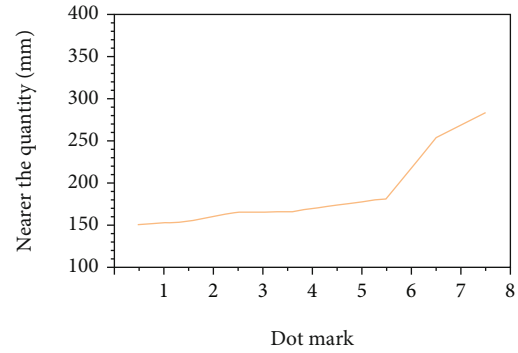

Figure 5: Moving quantity of two sides of auxiliary transportation.

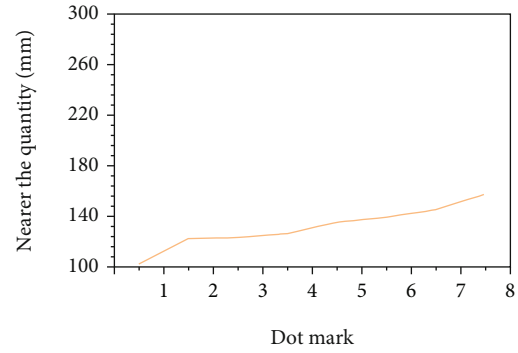

Figure 6: Top and bottom plate displacements of auxiliary transportation.

was between 200 and 300 mm, and the maximum displacement of the roof and floor was between 150 and –180 mm. The weakening of the roof weakened the deformation of the 42106 auxiliary roadway.

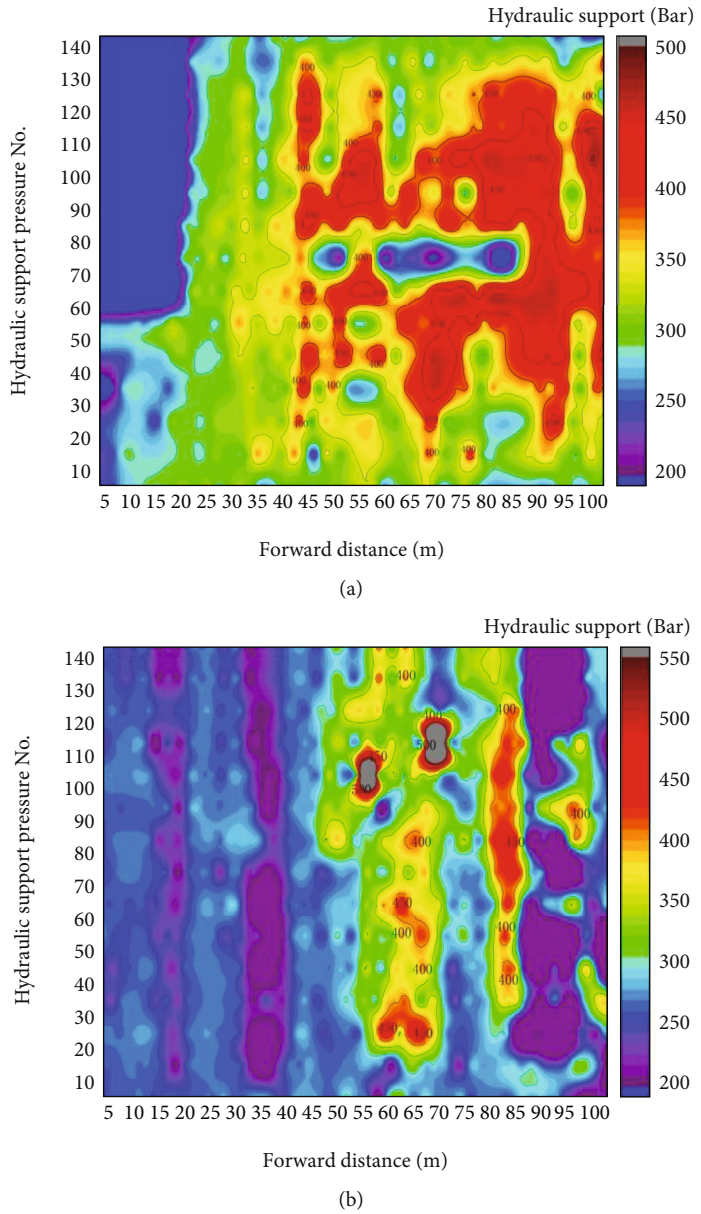

Figure 7: Comparison of the ore pressure law during initial production of the working face with and without hydraulic fracturing. (a) Mining pressure of 42106 working face during initial mining (no fracturing on the roof). (b) Mining pressure behavior of 42108 working face during initial mining (the roof has been fractured).

4.4. Stress Research of Roadway Surrounding Rock. According to the mine pressure monitoring results and early warning platform, the pressure strength of the 42106 working face was approximately 50 MPa without hydraulic fracturing. Meanwhile, after hydraulic fracturing of the 42108 working face roof, the working face pressure strength was reduced to approximately 35 MPa, and the periodic pressure step distance was reduced to weaken the roof effectively. Thus, the working face within the fracturing construction range was safely recovered, as shown in Figure 7.

The Figure 8 illustrates the change behavior of the average support load during the initial mining of the 42106 working face (roof unfractured), 42107 working face (roof fractured), and 42108 working face (roof fractured) in Buertai coal mine. The figure shows that under the same geological mining conditions, the average support load on the 42107 and 42108 working faces was lower than that on the 42106 working face: the average support load on the fully mechanized caving face with directional long borehole segmented hydraulic fracturing was lower than that without directional long borehole segmented hydraulic fracturing. The average load of the 42107 fully mechanized caving surface was 36.7 bar lower than that of the support of the 42106 fully mechanized caving surface and 59.12 bar lower than that of the support of the 42106 fully mechanized caving surface. The differences are equivalent to a decrease of 10.45% and 17.31%, respectively. Thus, directional long drilling segmented hydraulic fracturing can destroy the integrity of the

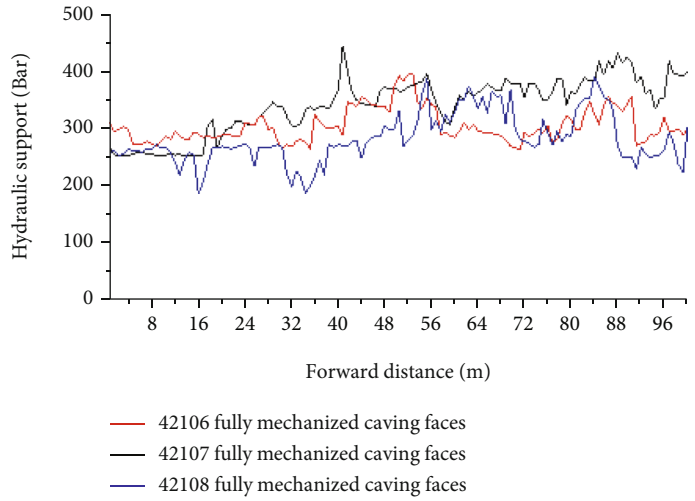

Figure 8: Comparison of average support load during initial production of fractured roof and unfractured working face.

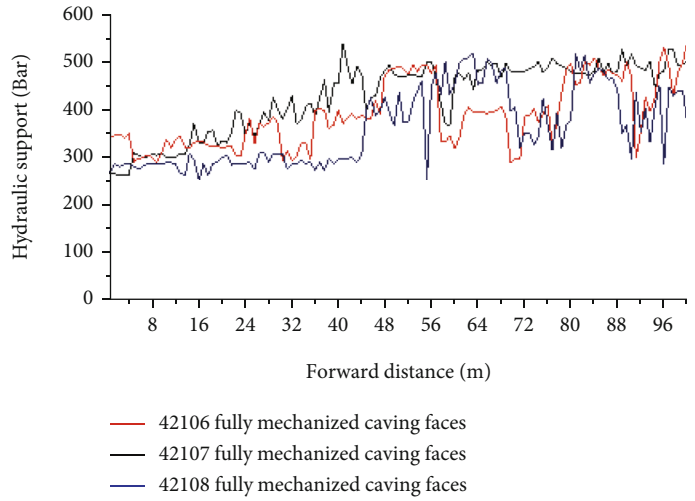

Figure 9: Comparison of maximum support load during initial production between fractured roof and unfractured working face.

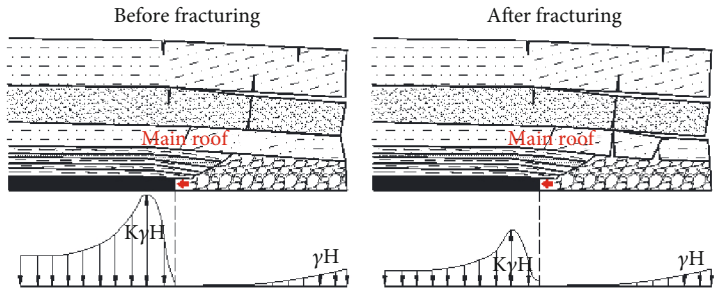

Figure 10: Reduction in advance abutment pressure after fracturing.

hard roof, reduce the ore pressure strength, and reduce the occurrence of strong ore pressure.

Figure 9 shows the variation in maximum support load during initial mining of the Buertai coal mine 42106 working face (roof unfractured), 42107 working face (roof fractured), and 42108 working face (fractured).

Figure 9 shows that under the same geological and mining conditions, the maximum load of the 42107 and 42108 fully mechanized face stents was less than that of the 42106 fully mechanized face stent. The implementation of the directional drilling long section of hydraulic fracturing deformation-failure support maximum load that did not

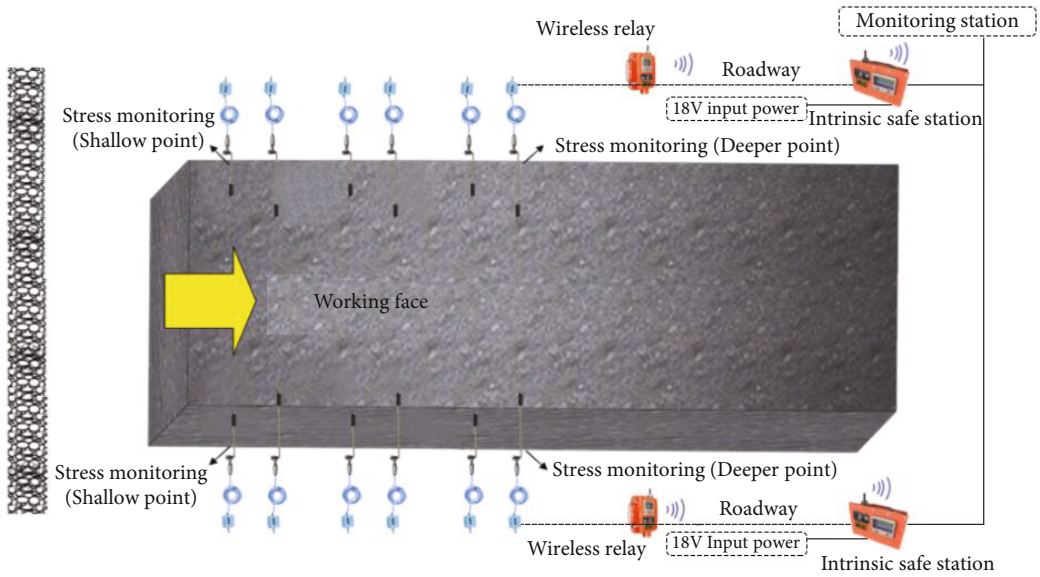

Figure 11: 42108 hardware composition and layout of monitoring equipment for top and bottom displacement of auxiliary transportation.

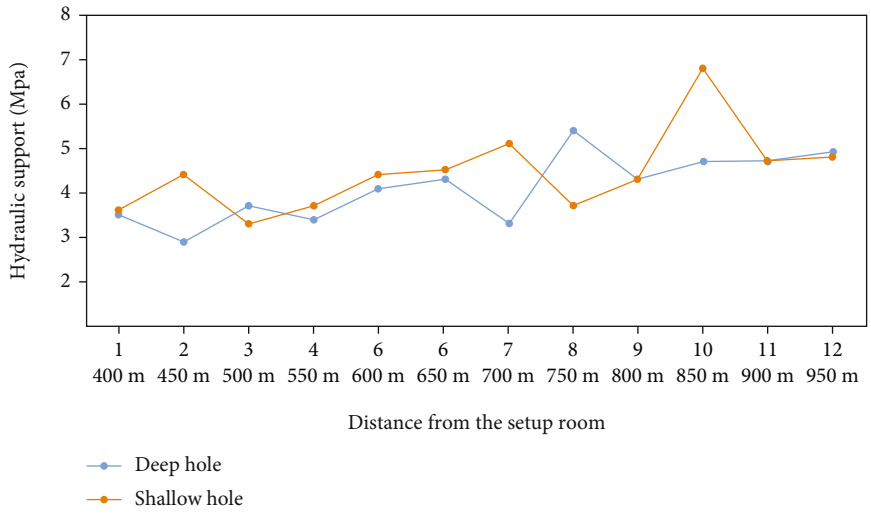

Figure 12: 42108 broken line chart of surrounding rock stress at the main auxiliary side.

implement the directional drilling section of hydraulic fracturing deformation-failure stent is low; the average load, during the preliminary extraction in the average maximum support load on the 42106 fully mechanized caving face, was 427.95 bar; that on the 42107 fully mechanized caving face was 389.56 bar; and that on the 42108 fully mechanized caving face was 361.4 bar. The maximum load of the 42107 fully mechanized caving surface was 38.39 bar lower than that of the support of the 42106 fully mechanized caving surface, with a 15.56% decrease. The maximum load of the 42108 fully mechanized caving surface was 66.55 bar lower than that of the support of the 42106 fully mechanized caving surface, with a 8.97% decrease. It follows that the maximum load of the old top of the fully mechanized working face support with directional long drilling is smaller than that of the fully mechanized working face support without hydraulic fracturing. To avoid the occurrence of strong ore pressure, the hydraulic fracturing of the hard roof covered by the fully mechanized working surface with directional long borehole can reduce the ore pressure strength during the initial pressure of the old roof.

After the directional long drilling hydraulic fracturing, the basic roof (old roof) was completely weakened, and its strength and integrity were considerably reduced. As the working face advanced, the basic roof collapsed, preventing the generation of a long suspended roof and reducing the concentration of the advanced abutment pressure. The deformation of the roadway surrounding rock was thus alleviated, and the working resistance of the support was reduced and transferred to the interior of the working face, as illustrated in Figure 10.

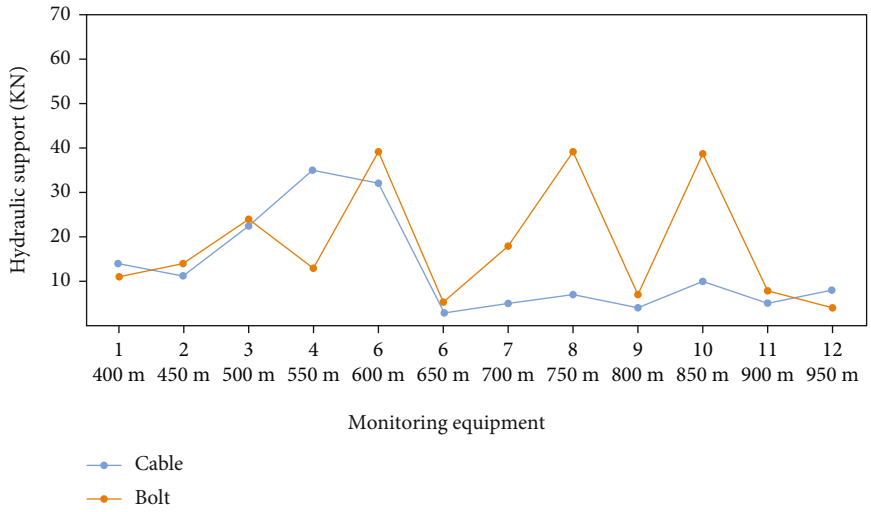

Figure 13: 42108 auxiliary side anchor cable/bolt stress line diagram.

4.5. Stress Monitoring and Analysis of Auxiliary Transport Trough

4.5.1. Analysis of Stress Monitoring Data of Normal Wall Rock. In 42108, several surrounding rock stress monitoring equipment were installed on the side every 50 m at the 400 m position of the auxiliary transport distance cut (two monitoring equipment were placed at each monitoring point: one deep base point (15 m) and one shallow base point (9 m)). Figure 11 illustrates the layout.

In this study, the stress values from 182–716 m of the fractured zone and 716–960 m of the unfractured zone were selected as the research objects, and the corresponding equipment points were from 1–12. The maximum stress values of each point are plotted as broken line charts in Figure 12.

The stress value of the deep hole from points 1–7 (400–700 m away from the cutting hole position and in the fracturing area of the roof) was between 3.5 and 5.5 MPa, and that of the shallow hole was between 4.5 and 5.3 MPa. The stress value of the deep hole from points 8–12 (750–950 m away from the cutting hole position in the roof unfractured area) was between 4.5 and 6.5 MPa, and that of the shallow hole was between 4.5 and 7.8 MPa. The weakening of the roof weakened the surrounding rock stress of auxiliary roadway 42108.

4.5.2. Stress Monitoring Analysis of Roof Side Anchor Cable/Bolt. In 42108, several anchor cable/bolt monitoring equipment were installed on the side every 50 m at the 400 m position of the auxiliary transport distance cutting hole (two monitoring equipment were placed at each monitoring point: one roof anchor cable monitoring and one auxiliary side anchor rod monitoring). For this analysis, stress values in the 182–716 m fractured area and 716–960 m unfractured area were selected as the research objects. The corresponding equipment point numbers were 1–12. The maximum stress value of each point is plotted as a broken line graph in Figure 13.

The stress value of the anchor cable at points 1–7 (400–700 m away from the cutting hole and in the fractured area of the roof) was 15–45 kN, the stress value of the anchor bolt was 15–50 kN, and the stress value of the anchor cable at points 8–12 (750–950 m away from the cutting hole and in the unfractured area of the roof) was 15–20 kN. The stress value of the anchor bolt was between 18 and 50 kN, and the stress value of the anchor cable decreased considerably after passing through the roof fracturing zone. However, the anchor bolt fluctuation increased after passing through the roof fracturing zone. The weakening of the roof weakened the surrounding rock stress of the 42108 auxiliary transport roadway and dispersed the surrounding rock stress of the auxiliary wall.

5. Conclusion

We used a mine pressure monitoring system to dynamically monitor roof support resistance and collect real-time support pressure data. Thus, we compared the data of the mining pressure characteristic before and after mining of the fracturing construction area and data of the surrounding rock stress monitoring. The conclusions of the study are summarized as follows:

(1) After fracturing, the overall pressure strength in the area affected by fracturing drilling in the working face was reduced, especially when the peak pressure decreased considerably by approximately 10%; the pressure step distance decreased by 4%, the support average resistance before fracturing decreased by 2.6%, and the support average resistance during fracturing decreased by 6.8%.

(2) After fracturing, the dynamic load coefficient was 4% lower than that of the unfractured area, the roadway deformation reduced, and the coal wall was restrained

(3) After the directional long drilling hydraulic fracturing, the basic roof (old roof) was completely weakened,

and its strength and integrity were considerably reduced. As the working face advanced, the basic roof energy collapsed, preventing the generation of long suspended roof and reducing the concentration of advanced abutment pressure. The deformation of the roadway surrounding rock was alleviated, and the support working resistance became low and transferred to the inside of the working face

(4) Before and after fracturing, the maximum stress value of the deep and shallow holes was reduced by approximately 1 MPa and 1.3 MPa, respectively, and the maximum stress value of the anchor cable was reduced by approximately 25 kN. The stress value of the anchor bolt was weakened, showing the effectiveness of the fracturing weakening effect

Data Availability

The data used to support the findings of this study are included within the article.

Conflicts of Interest

There is no conflicts of interest in the publication of this paper.

Acknowledgments

This work was supported by China Coal Technology Engineering Group Co., Ltd. (2019-2-ZD003) and the National Natural Science Foundation of China (52174188).

References

[1] J. Tang, *Study on Coal Seam Gas Migration Rule and Engineering Application under Hydraulic Fracturing*, General Institute of Coal Science, 2019.

[2] L. Y. Shuaifeng, W. A. Shengwei, Z. H. Xiaofei, L. I. Rui, H. E. Junhua, and H. U. Qi, "Pollution characteristics and evaluation of solid-phase materials in CBM drilling," *Coal geology & exploration*, vol. 45, no. 1, pp. 162–167, 2017.

[3] X. Liu, "Influencing factors of hydraulic propped fracture conductivity in shale reservoir," *Fault-Block Oil & Gas Field*, vol. 27, no. 3, pp. 394–398, 2020.

[4] L. Zhou and M. Z. Hou, "A new numerical 3D-model for simulation of hydraulic fracturing in consideration of hydro-mechanical coupling effects," *International Journal of Rock Mechanics and Mining Sciences*, vol. 60, no. 12, pp. 370–380, 2013.

[5] H. Chen, Z. Li, Z. Gao, and Y. Sun, "Numerical investigation of rock breaking mechanisms by high pressure water jet," *Procedia Engineering*, vol. 126, no. 10, pp. 295–299, 2015.

[6] Y. Lu, "Application of hydraulic fracturing technology in high gas and low permeability mine," *Journal of Chongqing University*, vol. 33, no. 7, pp. 102–107, 2010.

[7] Q. W. Guo, W. Han, W. Y. Zhang, X. B. Wang, and X. L. Hao, "Study on mechanism and application of hydraulic fracturing and permeability improvement gas drainage in underground mine," *Coal Science and Technology*, vol. 39, no. 12, pp. 60–64, 2011.

[8] Z. Sun, Z. Zhang, and Z. Wang, "Application & research on hydraulic fracturing and cutting top pressure relief technology in large mining height retained roadway," *Coal Science and Technology*, vol. 47, no. 10, pp. 190–197, 2019.

[9] X. M. Sun, X. Liu, G. F. Liang, D. Wang, and Y. L. Jiang, "Key parameters of gob-side entry retaining formed by roof cut and pressure releasing in thin coal seams," *Chinese Journal of Rock Mechanics and Engineering*, vol. 33, no. 7, pp. 1449–1456, 2014.

[10] B. Yu and H. Duan, "Study of roof control by hydraulic fracturing in full-mechanized caving mining with high strength in extra-thick coal layer," *Chinese Journal of Rock Mechanics and Engineering*, vol. 33, no. 7, pp. 778–785, 2014.

[11] S. Yan, Y. Ning, L. Kang, Y. Shi, Y. Wang, and Y. Li, "The mechanism of hydrobreakage to control hard roof and its test study," *Mei T'an Hsueh Pao (Journal of China Coal Society)*, vol. 25, no. 1, pp. 32–35, 2000.

[12] X. Zhang, "Study on the technology of hydraulic fracturing on the first roof caving of fully mechanized mining ace," *Coal Science and Technology*, vol. 45, no. 7, pp. 23–26, 2017.

[13] S. Ren and L. Sun, "Application of hydraulic fracturing technology in the initial roof release of fully mechanized mining face," *Coal Engineering*, vol. 49, no. S2, pp. 81–84, 2017.

[14] X. Meng and H. Zhao, "Study on hydraulic fracturing roof control technology for fully mechanized working face," *Coal Engineering*, vol. 49, no. 7, pp. 75–77, 2017.

[15] B. Wei, "Application on hydraulic fracturing technique in first caving of shallow buried coal seam," *Coal Science and Technology*, vol. 46, no. S1, pp. 100–102, 2018.

[16] C. Zhang, *Application Research of Hydraulic Fracturing Prevention and Treatment of Rock Burst*, Anhui University of Science and Technology, 2016.

[17] Z. Ouyang, Q. Qi, and Y. Zhang, "Mechanism and test of hydraulic fracturing to prevent rock burst," *Journal of Coal Science and Engineering (China)*, vol. 36, no. S2, pp. 321–325, 2011.

[18] X. Guo, *Mechanism and Experimental Research on Prevention and Treatment of Rock Burst by Ultra-High Pressure Hydraulic Fracturing of Coal Seam*, China University of Mining and Technology (Beijing), 2015.

[19] X. Zhang, "Application of hydraulic fracturing technology in the prevention and treatment of rock burst," *Coal Mine Safety*, vol. 41, no. 8, pp. 51-52, 2010.

[20] L. Wang, B. Meng, and Y. Cao, "Hydraulic fracturing volume opening model," *Journal of rock mechanics and engineering*, vol. 39, no. 5, pp. 887–898, 2020.

[21] B. Liang, L. Yue, and W. Sun, "The influence of shale mineral composition on crack growth: numerical simulation," *Marine and Petroleum Geology*, vol. 24, no. 4, pp. 97–101, 2019.

[22] H. Wang, H. Liu, J. Zhang, H. A. Wu, and X. X. Wang, "Numerical simulation of hydraulic fracture height control with different parameters," *Journal of University of Science and Technology of China*, vol. 41, no. 9, pp. 820–825, 2011.

[23] H. Kang and Y. Feng, "Hydraulic fracturing technology and its applications in strata control in underground coal mines," *Coal Science and Technology*, vol. 45, no. 1, pp. 1–9, 2017.

[24] Y. T. Guo, C. H. Yang, C. G. Jia, J. B. Xu, L. Wang, and D. Li, "Research on hydraulic fracturing physical simulation of shale and fracture characterization methods," *Chinese Journal of Rock Mechanics and Engineering*, vol. 33, no. 1, pp. 52–59, 2014.

[25] Y. Li, "Long multi-point underground directional drilling hydraulic fracturing technology for lowpermeability weak coalbed," *Safety in Mines*, vol. 49, no. 6, pp. 45–48, 2018.

[26] Y. Feng and H. Kang, "Control of hard and difficult roof cracking in coal mine by direct hydraulic fracture," *Journal of Rock Mechanics and Engineering*, vol. 31, no. 6, 2012.

[27] X. Liu, S. Zhang, and H. Guo, "A study on hydraulic fracturing technology of long drilling hole in coal mine," *Coal Science and Technology*, vol. 42, no. 3, pp. 42–44, 2014.

[28] G. P. Kang and Y. J. Feng, "Monitoring of stress change in coal seam caused by directional hydraulic fracturing in working face with strong roof and its evolution," *Journal of China Coal Society*, vol. 37, no. 12, pp. 1953–1959, 2012.

[29] R. Guo, *Study on Pressure Law and Control Technology of Fully Mechanized Caving Face with Low Mining and Caving Ratio in Bourtai Coal Mine*, Xi 'an University of Architecture and Technology, 2018.

[30] L. Qiu, Z. Liu, E. Wang, X. He, J. Feng, and B. Li, "Early-warning of rock burst in coal mine by low-frequency electromagnetic radiation," *Engineering Geology*, vol. 2020, article 105755, no. 279, 2020.

[31] Y. Liu, H. Wang, Q. Qi, A. Wang, and Y. Zhao, "Dynamic evolution law of overburden rock in shallow-buried super-high fully mechanized working face and determination of support strength," *Shock and Vibration*, vol. 2021, Article ID 7649459, 2021.

[32] L. M. Qiu, Y. Zhu, D. Song et al., "Study on the nonlinear characteristics of EMR and AE during coal splitting tests," *Minerals*, vol. 12, no. 2, p. 108, 2022.

[33] Y. Liu, Q. Qi, and A. Wang, "Influence of valleys terrain on pressure of fully mechanized working faces in shallow coal seams," *Shock and Vibration*, vol. 2021, Article ID 88800041, 2021.

[34] W. Luo, J. Yang, and Z. Gao, "Research and application of directional long- borehole staged hydraulic fracturing technology for strong rock pressure in mine," *Coal Science and Technology*, vol. 46, no. 11, pp. 43–49, 2018.